Astronomy & Astrophysics

Ammonia (*J,K*) = (1,1) to (4,4) and (6,6) inversion lines detected in the Seyfert 2 galaxy NGC 1068

Y. Ao[1,2], C. Henkel[1], J. A. Braatz[3], A. Weiß[1], K. M. Menten[1], and S. Mühle[4]

[1] MPIfR, Auf dem Hügel 69, 53121 Bonn, Germany
    e-mail: ypao@mpifr-bonn.mpg.de
[2] Purple Mountain Observatory, Chinese Academy of Sciences, Nanjing 210008, PR China
[3] National Radio Astronomy Observatory, 520 Edgemont Rd., Charlottesville, VA 22903, USA
[4] Joint Institute for VLBI in Europe, Postbus 2, 7990 AA Dwingeloo, The Netherlands

ABSTRACT

We present the detection of the ammonia (NH_3) (J,K) = (1,1) to (4,4) and (6,6) inversion lines toward the prototypical Seyfert 2 galaxy NGC 1068, made with the Green Bank Telescope (GBT). This is the first detection of ammonia in a Seyfert galaxy. The ortho-to-para-NH_3 abundance ratio suggests that the molecule was formed in a warm medium of at least 20 K. For the NH_3 column density and fractional abundance, we find $(1.09 \pm 0.23) \times 10^{14}$ cm^{-2} and $(2.9 \pm 0.6) \times 10^{-8}$, respectively, from the inner ~1.2 kpc of NGC 1068. The kinetic temperature can be constrained to 80 ± 20 K for the bulk of the molecular gas, while some fraction has an even higher temperature of 140 ± 30 K.

Key words. galaxies: individual: NGC 1068 – galaxies: Seyfert – galaxies: ISM – ISM: molecules – radio lines: galaxies

1. Introduction

Studies of molecular gas provide information about the gas density, the temperature, and kinematics within galaxies, help us to understand chemical evolution over cosmic time and allow us to study the triggering and fueling mechanisms of star formation and active galactic nuclei (AGN). Most stars are formed in dense gas cores, which are embedded in giant molecular clouds (GMCs). The star-forming activity is related to the dense gas and not to the bulk of the GMC's material (Gao & Solomon 2004). Determining the physical properties of the dense gas in galaxies is therefore of fundamental importance for our understanding of star formation and the evolution of galaxies. Among the most commonly observed species are CO, CS, HCN, and HCO$^+$. In local dark clouds, the temperature can be constrained by observations of the $J = 1-0$ transition of CO, both because this transition is opaque and thermalized and because the emission is often extended enough to fill the beam of a single-dish telescope. However, in external galaxies, filling factors are much less than unity. Furthermore, CO, CS, HCN, and HCO$^+$ suffer from a coupled sensitivity to the kinetic temperature and spatial density, making an observed line ratio consistent with both a high density at a low temperature and a low density at a high temperature. Specific information about the individual physical parameters therefore requires a molecular tracer that possesses a singular sensitivity to either density or temperature. Ammonia (NH_3) is such a molecule.

Ammonia is widespread and its level scheme contains inversion doublets owing to the tunneling of the nitrogen atom through the plane defined by the three hydrogen atoms. The metastable ($J, K = J$) rotational levels, for which the total angular momentum quantum number J is equal to its projection on the molecule's symmetry axis, are not radiatively but collisionally coupled. NH_3 is therefore a good tracer of the gas kinetic

temperature. Another advantage is that the inversion lines are quite close in frequency, thus allowing us to measure sources with similar beam sizes and to use the same telescope-receiver combination, which minimizes calibration uncertainties of the measured line ratios. As a consequence, NH_3 is widely studied to investigate the physical properties of dark clouds and massive star-forming regions in our Galaxy (e.g., Ho & Townes 1983; Walmsley & Ungerechts 1983; Bourke et al. 1995; Ceccarelli et al. 2002; Pillai et al. 2006; Wilson et al. 2006). However, in spite of the high sensitivity and stable baselines of present state-of-the-art facilities, ammonia multilevel studies in extragalactic sources are still rare and are limited to the Large Magellanic Cloud, IC 342, NGC 253, M 51, M 82, Maffei 2, and Arp 220 (Martin & Ho 1986; Henkel et al. 2000; Weiß et al. 2001; Takano et al. 2002; Mauersberger et al. 2003; Ott et al. 2005, 2010; Takano et al. 2005) in the local Universe, and in absorption to the gravitationally lensed B0218+357 and PKS 1830−211 at redshifts of $z \sim 0.7$ and 0.9 (Henkel et al. 2005, 2008).

NGC 1068, a prototypical Seyfert 2 galaxy (Antonucci & Miller 1985), is located at a distance of 15.5 Mpc (a heliocentric systemic velocity $cz = 1137$ km s^{-1} is used throughout this paper, adopted from the NASA/IPA Extragalactic Database), making it one of the nearest Seyfert galaxies and thus an ideal target to investigate the physical properties of the molecular gas in the vicinity of an AGN. Here we report the first detection of ammonia in this prominent Seyfert 2 galaxy to evaluate the kinetic temperature of its dense molecular gas.

2. Observations

We observed ammonia inversion lines toward the nucleus of NGC 1068 with the Green Bank Telescope (GBT) of the

National Radio Astronomy Observatory[1] on 2005 October 14 and October 19. We configured the telescope to observe both circular polarizations simultaneously using a total-power nodding mode in which the target position was placed alternately in one of the two beams of the 22−26 GHz K-band receiver. The full-width-at-half-maximum (*FWHM*) beam size was approximately 31″ in the observed frequency range, between 23.6 and 25.0 GHz. The pointing accuracy was ∼5″. To observe the $NH_3(1,1)$ through (4,4) lines, we configured the spectrometer with an 800 MHz spectral window centered on the $NH_3(3,3)$ line. The channel spacing was 390 kHz, corresponding to ∼5 $km\,s^{-1}$. We averaged the data from the two dates to produce the final spectrum, which has an on-source integration time of 4 h. We observed the $NH_3(6,6)$ line only on the second date, 2005 October 19. Here we used a 200 MHz spectral window observed with a channel spacing of 24 kHz, and then averaged channels in post-processing to achieve 390 kHz channel spacing. The total integration time for the $NH_3(6,6)$ line was 1 h.

The data were calibrated and averaged in GBTIDL. For calibration, we used an estimate of the atmospheric opacity obtained from a weather model. We subtracted a polynomial baseline fitted to the line-free channels adjacent to each ammonia line. For the (1,1) to (4,4) lines observed simultaneously, the relative calibration is very good and is limited primarily by the uncertainty in the baseline fits, which is 10% for the (1,1) to (3,3) lines, 15% for the (4,4) line, and 27% for the (6,6) line, respectively. The (1,1) and (2,2) line profiles are close to each other but are marginally separated and the Gaussian fit for each line does not suffer from this effect. With the calibration error of 15% for the GBT telescope itself, we estimate the absolute calibration uncertainties, including the error from the baseline fits, to be ∼18−31% for the ammonia lines.

3. Results

3.1. NH₃ lines

This is the first time that ammonia is detected in NGC 1068, making it the first Seyfert galaxy observed in this molecule. Also, because Arp 220, B0218+357, and PKS 1830-211 were detected in absorption, NGC 1068 is so far the most distant galaxy where ammonia is detected in emission. Three para, $(J, K) = (1,1)$, (2,2), and (4,4), and two ortho, $(J, K) = (3,3)$ and (6,6), transitions are covered by the observations, and all five are detected. Figure 1 shows the spectra before and after subtracting a polynomial baseline to the line free channels. The line parameters are listed in Table 1, where integrated flux, I, peak flux density, S, central velocity, V, and line width, $\Delta V_{1/2}$, are obtained from the results of Gaussian fitting.

The line profiles are similar for the (1,1), (2,2) and (3,3) lines, which share a similar central velocity of around −35 $km\,s^{-1}$, relative to a heliocentric systemic velocity of $cz = 1137$ $km\,s^{-1}$, and a *FWHM* line width of 220−274 $km\,s^{-1}$. The similar central velocities and the comparable widths of the (1,1), (2,2) and (3,3) lines suggest that the line emission comes from the same region. The (4,4) and (6,6) lines have different central velocities and a narrower line width. The (4,4) line is located at a frequency where the baseline is particularly steep. The (6,6) line is weak and falls into a window with a slightly
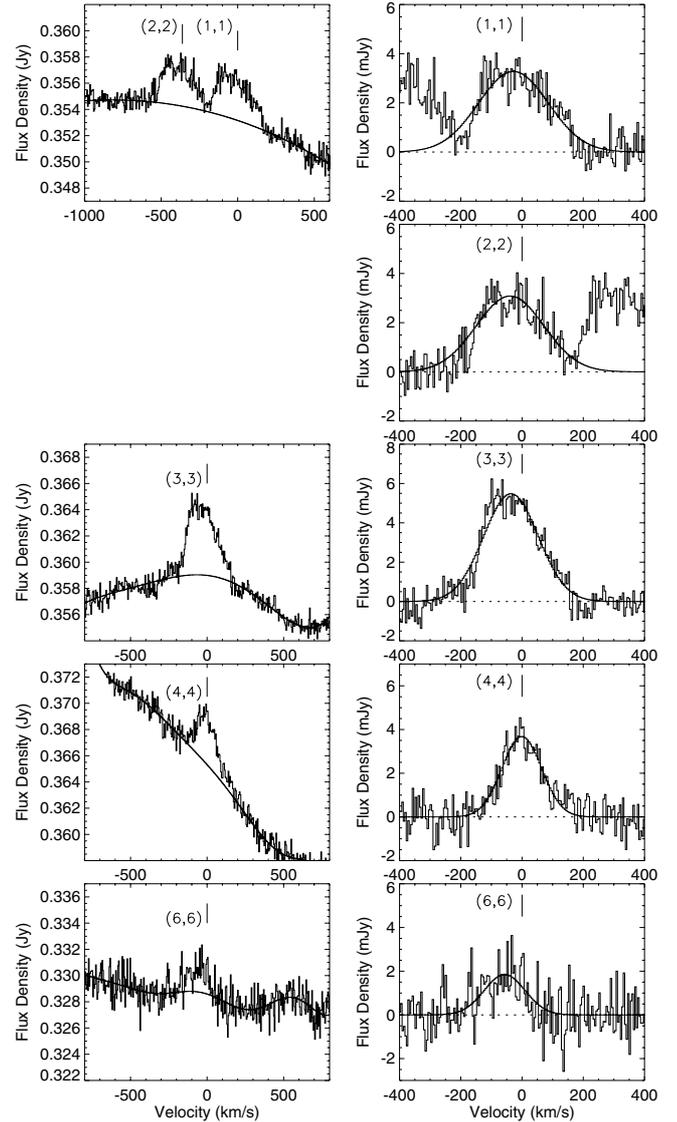
Fig. 1. Metastable ammonia inversion lines observed toward NGC 1068 ($\alpha_{2000} = 02^h42^m40.7^s$, $\delta_{2000} = -00^o00'48''$). Vertical lines mark a heliocentric systemic velocity of $cz = 1137$ $km\,s^{-1}$. Velocities are displayed relative to this value (in the upper left panel, the velocity scale refers to the (1,1) line). *Left*: spectra without baseline subtraction, overlaid with a polynomial baseline fit to the line-free channels. *Right*: final baseline-subtracted spectra overlaid with Gaussian fits.

distorted baseline, making it difficult to determine accurate line parameters. The comparatively narrow line widths of the (4,4) and (6,6) lines may suggest that their emission originates from a less extended region than that of the lower excitation lines.

Our measured continuum flux density of NGC 1068 ranges from 0.33 to 0.37 Jy at frequencies of 23.4 to 25.1 GHz. This is consistent with the value of 0.342 ± 0.034 at 22 GHz reported by Ricci et al. (2006).

3.2. NH₃ column density and rotation temperature

Assuming that the line emission is optically thin and the contribution from the cosmic background is negligible, the sum of the

Table 1. NH$_3$ line parameters.

(J,K)	I^a (Jy km s^{-1})	S^a (mJy)	V^a (km s^{-1})	$\Delta V_{1/2}^a$ (km s^{-1})	$N(J, K)^b$ (10^{13} cm^{-2})
(1,1)	0.89(0.07)	3.26(0.13)	−30(6)	274(17)	2.52(0.24)
(2,2)	0.79(0.06)	3.10(0.14)	−37(6)	254(19)	1.67(0.19)
(3,3)	1.19(0.10)	5.40(0.14)	−37(3)	220(8)	2.22(0.13)
(4,4)	0.55(0.05)	3.72(0.14)	−2(3)	149(7)	0.96(0.07)
(6,6)	0.28(0.04)	1.88(0.23)	−56(9)	147(27)	0.43(0.12)
(5,5)					0.53
(0,0)					2.55
N_{total}					10.9(2.3)

Notes. $^{(a)}$ The values are derived from Gaussian fits to the spectra. Given velocities are relative to a heliocentric velocity of $cz = 1137$ km s^{-1}. $^{(b)}$ The column density for the (5,5) state is extrapolated from the (2,2) and (4,4) states using $T_{\text{rot}} = 119$ K, while the value for the (0,0) state is extrapolated from the (3,3) state by adopting $T_{\text{rot}} = 44$ K. The total column density, N_{total}, includes the populations of the levels from (0,0) to (6,6). Because relative calibration is excellent up to at least the (4,4) transition, the errors given in parenthesis refer exclusively to the Gaussian fits. For the cumulative column density, N_{total}, however, the given error accounts for the absolute calibration uncertainty (Sect. 2).

beam-averaged column densities of the two states of an inversion doublet can be calculated using

$$N(J, K) = \frac{1.55 \times 10^{14}}{\nu} \frac{J(J+1)}{K^2} \int T_{\text{mb}} dv \qquad (1)$$

(e.g., Mauersberger et al. 2003), where the column density $N(J, K)$, the frequency ν, and the integrated line intensity $\int T_{\text{mb}} dv$, based on the main beam brightness temperature, T_{mb}, are in units of cm^{-2}, GHz, and K km s^{-1}, respectively. The calculated column densities (1 Jy corresponds to 2.16 K on a T_{mb} scale^2) are given in Table 1.

Following the analysis described by Henkel et al. (2000), the rotational temperature (T_{rot}) between different energy levels can be determined from the slope, a, of a linear fit in the rotation diagram (i.e., Boltzmann plot, which is normalized column density against energy above the ground state expressed in E/k) by $T_{\text{rot}} = -\log e/a \approx -0.434/a$. Figure 2 shows the rotation diagram including the five measured metastable NH$_3$ inversion lines. Ignoring differences in line shape, we obtain $T_{\text{rot}} = 92^{+29}_{-18}$ K by fitting the para-NH$_3$ species, i.e. the (1,1), (2,2) and (4,4) transitions, and $T_{\text{rot}} = 125^{+11}_{-8}$ K for the (3,3) and (6,6) ortho-NH$_3$ transitions. As discussed in Sect. 3.1, the (1,1), (2,2) and (3,3) line emission may originate in a region that is different from that of the (4,4) and (6,6) lines. The former three lines can be fitted by $T_{\text{rot}} = 61^{+12}_{-9}$ K, and the latter two by $T_{\text{rot}} = 111^{+12}_{-9}$ K. The rotation temperature between the lowest inversion doublets of para-ammonia, (1,1) and (2,2), is $T_{\text{rot}} = 44^{+6}_{-4}$ K. Without the (1,1) state, the other two para-NH$_3$ transitions, (2,2) and (4,4), yield $T_{\text{rot}} = 119^{+15}_{-11}$ K.

3.3. NH$_3$ abundance

To estimate the populations of the $(J, K) = (0,0)$ and (5,5) states, we assume the rotation temperature $T_{\text{rot}} = 44$ K, derived from the two lowest inversion doublets, for the (0,0) ground state, and $T_{\text{rot}} = 119$ K from the fit to the (2,2) and (4,4) lines, for the (5,5) state. The derived column densities are 2.55×10^{13} cm^{-2} for the (0,0) state, which is not a doublet, and 0.53×10^{13} cm^{-2} for the (5,5) state, respectively. The former is extrapolated from the (3,3) state and the latter from the (2,2) and (4,4) states. The
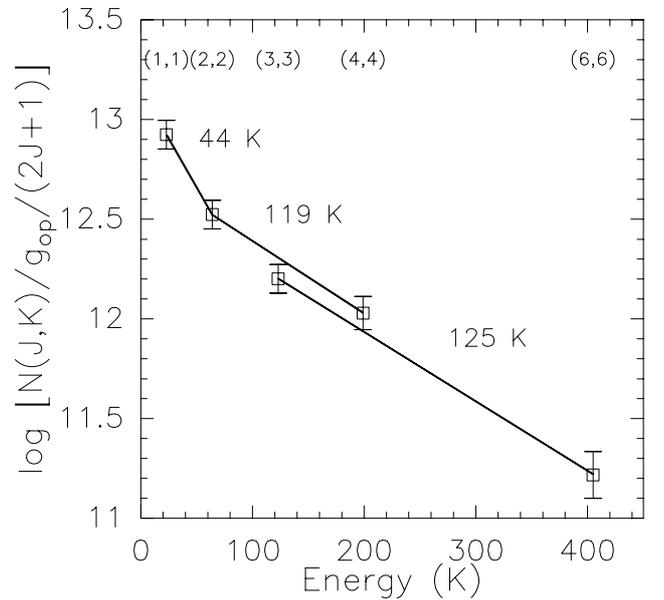
Fig. 2. Rotation diagram of metastable ammonia transitions toward NGC 1068 (see Sect. 3.2). The open squares show the normalized column densities determined from the integrated line intensities. The numbers mark the rotational temperatures in K. The absolute calibration uncertainties, including the dominant contribution from the baseline fits as well as uncertainties in the Gaussian fits and in the overall calibration uncertainty, have been taken as error bars (Sect. 2). Note, however, that relative calibration is excellent up to at least the (4,4) transition.

resulting total column density of ammonia is $(1.09 \pm 0.23) \times 10^{14}$ cm^{-2} if only considering the populations in the metastable states up to $(J, K) = (6,6)$. This yields an ammonia gas mass of $68 \pm 14\ M_\odot$ within a beam size of 31″, which corresponds to a physical size of 2.3 kpc. To estimate the mass of molecular gas in NGC 1068, we convolved the 17″ resolution map in CO $J = 1-0$ by Kaneko et al. (1989) to the GBT's resolution of 31″ and derived an integrated intensity of 103 K km s^{-1}. Adopting a conversion factor of 0.8 $M_\odot$ (K km s^{-1} pc^2)$^{-1}$, which describes ultraluminous galaxies (Downes & Solomon 1998) and less conspicuous nuclear starbursts (Mauersberger et al. 2003), we obtain a molecular gas mass of $3.5 \times 10^8\ M_\odot$. Therefore, the ammonia abundance relative to molecular hydrogen is estimated to
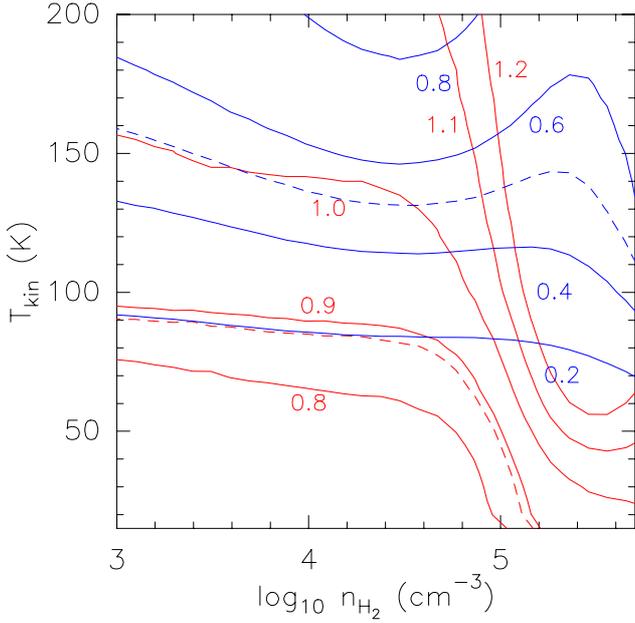
Fig. 3. NH$_3$ inversion line ratios as a function of the H$_2$ density (n_{H_2}) and kinetic temperature (T_{kin}). The red and blue lines mark the (2,2)/(1,1) and (6,6)/(4,4) line ratios, respectively, obtained from the large velocity gradient model outlined in Sect. 4. Dashed lines show the line ratios measured with the GBT. [NH$_3$]/(dv/dr) = 10^{-8} pc (km s^{-1})$^{-1}$ ([NH$_3$] = N(NH$_3$)/N(H$_2$) is the fractional abundance of ammonia). At high densities the (1,1) and (2,2) lines saturate, which causes the steeply declining T_{kin} values with rising density for a given (2,2)/(1,1) line ratio.

be $(2.9 \pm 0.6) \times 10^{-8}$ within a radius of ~1.2 kpc around the center of NGC 1068.

4. Discussion

The ammonia abundance in NGC 1068 is consistent with the values of $(1.3-2.0) \times 10^{-8}$ reported by Mauersberger et al. (2003) for the central regions of several nearby galaxies such as NGC 253, Maffei 2 and IC 342. It is lower than that of a few $\times 10^{-7}$ for the central ~500 pc of the Milky Way (Rodríguez-Fernández et al. 2001), but higher than the extremely low value of 5×10^{-10} determined for M 82 by Weiß et al. (2001). M 82 is a special case, because it contains a starburst in a late stage of its evolution leaving NH$_3$, which is a molecule particularly sensitive to UV radiation (e.g., Suto & Lee 1983), in only a few molecular cores that are still sufficiently shielded against the intense radiation field.

With the three para- and two ortho-NH$_3$ lines observed, we can estimate the ortho-to-para abundance ratio to be $R \sim 0.9$ (we do not give an error here because of the extrapolated (0,0) column density) as an upper limit because the (0,0) column density might be overestimated by extrapolating from the (3,3) column density, which could be affected by maser activity (e.g., Walmsley & Ungerechts 1983; Ott et al. 2005). A value near or below unity is expected, if ammonia was formed in a warm medium at a gas kinetic temperature of at least 20 K and only R values above ~1.5 would hint at a cool formation temperature of ~20 K (e.g., Takano et al. 2002).

The rotation temperatures from the multilevel study of the ammonia inversion lines are a good approximation to the kinetic gas temperature only for low ($T_{kin} \leq 20$ K) temperatures (Walmsley & Ungerechts 1983; Danby et al. 1988). At higher temperatures, the rotation temperature provides a robust lower

limit to the kinetic gas temperature as long as saturation effects do not play a role.

To determine the kinetic temperature itself, we here use a one-component large velocity gradient (LVG) analysis adopting a spherical cloud geometry as described by Ott et al. (2005). Dahmen et al. (1998) estimated that the velocity gradient ranges from 3 to 6 km s^{-1} pc^{-1} for Galactic center clouds and Meier et al. (2008) found a typical value of 1 to 2 km s^{-1} pc^{-1} for GMCs. Here we adopt a median value of 3 km s^{-1} pc^{-1} for the LVG models presented in this paper. The ammonia abundance derived in Sect. 3.3 is adopted, which yields an NH$_3$ abundance per velocity gradient of [NH$_3$]/(dv/dr) ~ 10^{-8} pc (km s^{-1})$^{-1}$ ([NH$_3$] = N(NH$_3$)/N(H$_2$) is the fractional abundance of ammonia). Changing the velocity gradient by a factor of 3 will affect the derived kinetic temperature by less than 10 K. Figure 3 shows NH$_3$ inversion line ratios as a function of the H$_2$ density (n_{H_2}) and kinetic temperature (T_{kin}). As long as the NH$_3$ lines are optically thin, the ratios are almost independent of the gas density and are therefore a good indicator for gas kinetic temperature. At high densities the (1,1) and (2,2) lines saturate, which causes the steeply declining T_{kin} values with rising density for a given (2,2)/(1,1) line ratio. While the optical depth may be well above unity in molecular cores (see, Güsten et al. 1981 for the Galactic center region), the bulk of the ammonia emission should be optically thin and arises from gas densities $n_{H_2} < 10^5$ cm^{-3} (e.g., Tieftrunk et al. 1998). For a typical gas density, n_{H_2}, of $10^{3.0-4.8}$ cm^{-3}, the observed (2,2)/(1,1) line ratio constrains the kinetic temperature T_{kin} to 80 ± 20 K, which characterizes the bulk of the molecular gas. The (6,6)/(4,4) line ratio yields a gas temperature of 140 ± 30 K for a gas density within the range of $10^{3.0-5.5}$ cm^{-3}. The latter indicates the existence of a hotter component of the gas, as is also suggested by the high rotational temperature revealed by the rotation diagram (Fig. 2). Here the (6,6)/(3,3) line ratio is not used to estimate the temperature because the (3,3) line emission is partly affected by the maser activity in some parameter ranges (Walmsley & Ungerechts 1983), and because the (6,6) line was not observed simultaneously as the (3,3) line and the uncertainty of the baseline fit of the (6,6) line is largest among all spectra as described in Sect. 2.

The GBT beam size covers the two inner spiral arms and the circumnuclear disk (CND) of NGC 1068 (see, e.g., Schinnerer et al. 2000). Our observed ammonia line emission likely has contributions from the spiral arms and the CND. The CND may be warmer because it is heated not only by young stars but also by the AGN. There are observations that directly support higher temperatures in the CND. Infrared rotational transitions of molecular hydrogen (Lutz et al. 1997) indicate a wide range of gas temperatures between 100 and 800 K. The dust near the AGN has been particularly thoroughly studied (e.g., Tomono et al. 2006; Poncelet et al. 2007; Raban et al. 2009). Because densities may be high within the central arcsecond ($\gtrsim 10^5$ cm^{-3}), the dust and the gas phase may be coupled and thus these results may be relevant for the kinetic temperature of the gas component. With mid-infrared (MIR) multi-filter data, Tomono et al. (2006) obtained a dust temperature of ~200 K within a 1.0″–sized region (~80 pc).

Our data provide a direct estimate of the gas properties for molecular gas in the inner 1.2 kpc of the galaxy. However, higher angular resolution data are needed to separate the different components and to isolate the CND in this galaxy.

5. Conclusions

Our main results from the ammonia observations toward the prototypical Seyfert 2 galaxy NGC 1068 are:

(1) The metastable NH_3 $(J,K) = (1,1)$ to $(4,4)$ and $(6,6)$ inversion lines are for the first time detected in emission toward NGC 1068. This opens up a new avenue to determine kinetic temperatures of the dense gas in nearby highly obscured AGN.

(2) For the NH_3 column density and fractional abundance, we find $(1.09 \pm 0.23) \times 10^{14}$ cm^{-2} and $(2.9 \pm 0.6) \times 10^{-8}$ in the inner ~1.2 kpc of NGC 1068.

(3) With an ortho-to-para-NH_3 abundance ratio of ~0.9, the ammonia should have been formed in a warm medium of at least 20 K.

(4) The kinetic temperature can be constrained to 80 ± 20 K for the bulk of the molecular gas, while some gas fraction has an even higher temperature of 140 ± 30 K.

References

Antonucci, R. R. J., & Miller, J. S. 1985, ApJ, 297, 621
Bourke, T. L., Hyland, A. R., Robinson, G., James, S. D., & Wright, C. M. 1995, MNRAS, 276, 1067
Ceccarelli, C., Baluteau, J.-P., Walmsley, M., et al. 2002, A&A, 383, 603
Dahmen, G., Huttemeister, S., Wilson, T. L., & Mauersberger, R. 1998, A&A, 331, 959
Danby, G., Flower, D. R., Valiron, P., Schilke, P., & Walmsley, C. M. 1988, MNRAS, 235, 229
Downes, D., & Solomon, P. M. 1998, ApJ, 507, 615
Gao, Y., & Solomon, P. M. 2004, ApJ, 606, 271
Guesten, R., Walmsley, C. M., & Pauls, T. 1981, A&A, 103, 197
Henkel, C., Mauersberger, R., Peck, A. B., Falcke, H., & Hagiwara, Y. 2000, A&A, 361, L45
Henkel, C., Jethava, N., Kraus, A., et al. 2005, A&A, 440, 893
Henkel, C., Braatz, J. A., Menten, K. M., & Ott, J. 2008, A&A, 485, 451
Ho, P. T. P., & Townes, C. H. 1983, ARA&A, 21, 239
Kaneko, N., Morita, K., Fukui, Y., et al. 1989, ApJ, 337, 691
Lutz, D., Sturm, E., Genzel, R., Moorwood, A. F. M., & Sternberg, A. 1997, Ap&SS, 248, 217
Martin, R. N., & Ho, P. T. P. 1986, ApJ, 308, L7
Mauersberger, R., Henkel, C., Weiß, A., Peck, A. B., & Hagiwara, Y. 2003, A&A, 403, 561
Meier, D. S., Turner, J. L., & Hurt, R. L. 2008, ApJ, 675, 281
Ott, J., Weiss, A., Henkel, C., & Walter, F. 2005, ApJ, 629, 767
Ott, J., Henkel, C., Staveley-Smith, L., & Weiß, A. 2010, ApJ, 710, 105
Pillai, T., Wyrowski, F., Carey, S. J., & Menten, K. M. 2006, A&A, 450, 569
Poncelet, A., Doucet, C., Perrin, G., Sol, H., & Lagage, P. O. 2007, A&A, 472, 823
Raban, D., Jaffe, W., Röttgering, H., Meisenheimer, K., & Tristram, K. R. W. 2009, MNRAS, 394, 1325
Ricci, R., Prandoni, I., Gruppioni, C., Sault, R. J., & de Zotti, G. 2006, A&A, 445, 465
Schinnerer, E., Eckart, A., Tacconi, L. J., Genzel, R., & Downes, D. 2000, ApJ, 533, 850
Suto, M., & Lee, L. C. 1983, J. Chem. Phys., 78, 4515
Takano, S., Nakai, N., & Kawaguchi, K. 2002, PASJ, 54, 195
Takano, S., Hofner, P., Winnewisser, G., Nakai, N., & Kawaguchi, K. 2005, PASJ, 57, 549
Tieftrunk, A. R., Megeath, S. T., Wilson, T. L., & Rayner, J. T. 1998, A&A, 336, 991
Tomono, D., Terada, H., & Kobayashi, N. 2006, ApJ, 646, 774
Walmsley, C. M., & Ungerechts, H. 1983, A&A, 122, 164
Weiß, A., Neininger, N., Henkel, C., Stutzki, J., & Klein, U. 2001, ApJ, 554, L143
Wilson, T. L., Henkel, C., & Hüttemeister, S. 2006, A&A, 460, 533